R. Schädler[1]
Laboratory for Energy Conversion,
Department of Mechanical
and Process Engineering,
ETH Zurich,
Sonneggstrasse 3,
Zurich CH-8092, Switzerland
e-mail: schaedler@lec.mavt.ethz.ch

A. I. Kalfas
Department of Mechanical Engineering,
Aristotle University of Thessaloniki,
Thessaloniki GR-54124, Greece
e-mail: akalfas@auth.gr

R. S. Abhari
Laboratory for Energy Conversion,
Department of Mechanical
and Process Engineering,
ETH Zurich,
Sonneggstrasse 3,
Zurich CH-8092, Switzerland
e-mail: abhari@lec.mavt.ethz.ch

G. Schmid
Siemens AG,
Mellinghofer Str. 55,
Muelheim an der Ruhr D-45473, Germany
e-mail: gregor.schmid@siemens.com

S. Voelker
Siemens AG,
Mellinghofer Str. 55,
Muelheim an der Ruhr D-45473, Germany
e-mail: voelker.stefan@siemens.com

Modulation and Radial Migration of Turbine Hub Cavity Modes by the Rim Seal Purge Flow

In the present paper, the results of an experimental and numerical investigation of the hub cavity modes and their migration into the main annulus flow are presented. A one-and-a-half stage, unshrouded and highly loaded axial turbine configuration with three-dimensionally shaped blades and cylindrical end walls has been tested in an axial turbine facility. Both the blade design and the rim seal purge flow path are representative to modern high-pressure gas turbines. The unsteady flow field at the hub cavity exit region has been measured with the fast-response aerodynamic probe (FRAP) for two different rim seal purge flow rates. Furthermore, fast-response wall-mounted pressure transducers have been installed inside the cavity. Unsteady full-annular computational fluid dynamics (CFD) simulations have been employed in order to complement the experimental work. The time-resolved pressure measurements inside the hub cavity reveal clear cavity modes, which show a strong dependency on the injected amount of rim seal purge flow. The numerical predictions provide information on the origin of these modes and relate them to pronounced ingestion spots around the circumference. The unsteady probe measurements at the rim seal interface show that the signature of the hub cavity induced modes migrates into the main annulus flow up to 30% blade span. Based on that, an aerodynamic loss mechanism has been found, showing that the benefit in loss reduction by decreasing the rim seal purge flow rate is weakened by the presence of turbine hub cavity modes. [DOI: 10.1115/1.4034416]

Introduction

In modern high-pressure gas turbines, the ingestion of hot gas from the main annulus into the stator–rotor hub cavity has to be suppressed. Relatively cold air is bypassed from the compressor and guided through the rim seal purge flow path in order to lower the risk of local overheating of the rotor disk and fatigue failures. The goal is to achieve an increased life time and ensure safe operation combined with a low detrimental effect on gas turbine's efficiency by appropriately choosing the amount of injected rim seal purge flow.

Several studies have been published, which focus on the ingestion mechanisms of the turbine main annulus flow into the hub cavity. Johnson et al. [1] identified two dominant drivers for the phenomena. Ingestion due to rotor pumping forces the hot gas into the hub cavity due to the radial pressure gradient provoked by a local mass flow imbalance on stator and rotor sided cavity surface. Furthermore, the interaction of the nozzle guide vane and the rotor blades builds up a pronounced zone of high static pressure which triggers the ingress of the hot gas.

In order to increase the sealing effectiveness, several authors reported systematic variations of the rim seal geometry. Popović and Hodson [2,3] performed parametric, numerical, and experimental investigations of an overlapping rim seal design showing that smallest changes in the geometry affect the vortical structures at the exit of the rim seal. These structures were found to have a strong impact on the unsteady interaction between the rim seal purge flow and the main annulus flow.

The unsteady nature of the flow field inside the hub cavity has been focus of several numerical studies. Julien et al. [4] found low-frequency pressure fluctuations inside the cavity which have been associated to large-scale vortical structures. The energetic content of these structures has been reduced as the rim seal purge flow rate was increased which leads to a stabilization of the cavity pressure fluctuations. Boudet et al. [5] performed unsteady numerical simulations of a high-pressure gas turbine stage including hub cavity out of which they found a dominant cavity frequency at 44% of the rotor blade passing frequency (RBPF). The authors attributed this frequency to a flow structure driven by the competition of centrifugal forces and pressure gradient inside the cavity. Similar findings have been reported by Jakoby et al. [6]. The extensive numerical study is complemented by a set of experimental data that show pronounced low-frequency pressure fluctuations measured inside an axial rim seal cavity for purge flow rates below a certain limit. The authors concluded that these pronounced pressure fluctuations are not caused by the vane–blade interaction and have a significant contribution to the hot gas ingestion into the hub cavity. Chilla et al. [7] performed extensive numerical investigations of different overlap-type rim seal geometries and related the pronounced low-frequency pressure fluctuations at the rim seal interface to a vortex shedding process of the flow structures into the rotor hub end wall. The circumferential

[1]Corresponding author.

Contributed by the International Gas Turbine Institute (IGTI) of ASME for publication in the JOURNAL OF TURBOMACHINERY. Manuscript received July 18, 2016; final manuscript received August 2, 2016; published online September 20, 2016. Editor: Kenneth Hall.

nonuniform pressure field provoked by the rotor–stator interaction, the purge flow rate, the circumferential velocity difference between cavity flow and main annulus flow, as well as the rim seal geometry have been identified as main drivers for the instabilities found at the rim seal interface.

Schuepbach et al. [8] conducted time-resolved pressure measurements at the rotor exit of a 1.5-stage highly loaded axial turbine for two different rim seal purge flow rates. The spectral analysis of the pressure signal for purge flow injection revealed a band of elevated pressure fluctuations at around half of the rotor blade passing frequency, whereas the low-frequency content vanished by changing to nominal sucking. The authors associated the pronounced low-frequency pressure fluctuations to a nonlinear interaction with cavity instabilities.

Apart from various studies on the turbine hub rim seal cavity flow field, several authors reported on detailed investigations on the unsteady interaction of the rim seal purge flow with the main annulus flow. Specifically, the unsteady interaction of the purge flow and the hub passage vortex (HPV) of stators and rotors has been studied by Hunter and Manwaring [9] and Jenny et al. [10]. Several studies focus on the sensitivity of the aerodynamic efficiency to the injected amount of rim seal purge flow. Reid et al. [11] reported that the two sources of aerodynamic losses induced by the purge flow, mixing of the purge flow with the main annulus flow, and the strengthening of the secondary flow structures through the rotor, are equal in their loss contribution. Mclean et al. [12] found a strong dependency of the aerodynamic losses to the injection type when increasing the rim seal purge flow rate. Paniagua et al. [13] described in their work that the radial migration of the rotor hub passage vortex and the therefore associated losses are attributed to the lower temperature of the purge flow. Ong et al. [14] linked the strengthening and the increased penetration of the rotor hub passage vortex to the provoked negative incidence. The trade-off between providing sufficient cooling to the rotor disk and lowering the aerodynamic losses represents one of the major turbine design objectives in recent years.

Substantial amount of research has been done in terms of turbine hub cavity flow structures and the interaction mechanisms between the rim seal purge flow and the main annulus flow. The specific objectives of the present paper are to experimentally and numerically investigate the turbine hub cavity modes and trace their unsteady flow behavior into the main annulus flow in order to quantify their impact by means of radial migration and aerodynamic losses.

Experimental Method

The experimental investigation was performed in the research axial turbine facility "LISA" in the Laboratory for Energy Conversion (LEC) at ETH Zurich, Zurich, Switzerland. The test rig was assembled with a one-and-a-half stage, high-pressure turbine representative configuration including an unshrouded rotor and cylindrical end walls at hub and tip for all the three blade rows.

Research Turbine Facility. The test facility is designed in order to accommodate moderate speed and a low-temperature model of an axial turbine with nondimensional operating parameters that are matching real engine conditions. The air loop of the test rig is quasi-closed and includes a single-stage centrifugal compressor, a two-stage water-to-air heat exchanger controlling the turbine inlet temperature, and a calibrated venturi nozzle for accurate mass flow measurements. At the exit of the turbine test section, the air loop opens to atmosphere.

Upstream of the turbine test section is a 3-m long flow conditioning duct in order to ensure a homogenous flow field at the turbine inlet. Furthermore, the flow undergoes an acceleration ahead of the turbine to reduce the significance of any remaining flow nonuniformities from upstream. A DC generator absorbs the power of the turbine and controls the rotational speed with an indicated accuracy of $\pm 0.02\%$ (± 0.5 rpm). The total inlet temperature $T_{0,\text{in}}$ is controlled by the water-to-air heat exchanger to an accuracy of ± 0.3 K. In order to measure the torque on the rotor shaft, a torque meter is installed on the vertical shaft. Due to the limited pressure ratio $\pi_{c,\max} = 1.5$ of the centrifugal compressor, a tandem deswirl vane arrangement is installed in order to recover the static pressure back to ambient level at the exit of the second stator (S2), which allows to reach the intended pressure ratio of $\pi_{1.5} = 1.65$. The unshrouded rotor has a tip gap of 1% of the blade span, and the tip gap variations between different assemblies are less than 1% of the tip gap which provides good repeatability. At the exit of the first stator (S1), the main flow is compressible with an average exit Mach number of 0.53. The current turbine configuration is derived from the turbine design extensively presented by Behr et al. [15]. The increased blade row spacing between the first stator and rotor as well as an increased axial clearance at the exit of the hub cavity build the major differences. The airfoil designs of the tested axial turbine configuration have been explained in detail by Regina et al. [16].

Operating Conditions. In order to account for changes in the atmospheric pressure for different measurement days, the turbine's 1.5-stage total-to-static pressure ratio is kept constant at $\pi_{1.5} = 1.65$ during the measurements. The static pressure information given in this work are nondimensionalized by the respective inlet total pressure. Table 1 presents the key operating parameters and the geometrical characteristics.

During the experiments, the rim seal purge flow is continuously injected from the rotor upstream hub cavity along the full annulus. The necessary mass flow is an off-take from the primary air loop upstream of the flow conditioning stretch and is measured by a standard nozzle. The bypassed air is fed through ten nozzle guide vanes (Fig. 1, B) around the circumference into the cavity underneath the first stator (S1) hub platform. A schematic of the rim seal purge flow path is depicted in Fig. 1.

Once the bypassed air B has entered the hub cavity, the mass flow is separated by two different paths which are indicated by dotted arrows in Fig. 1 (left). The flow path labeled with P describes the injection of purge flow into the main annulus flow. The flow path labeled with S is termed secondary flow path and is ejected through the drum into atmosphere, after being measured by an additional standard nozzle.

The pressure difference across the rotor downstream rim seal is controlled to be zero during the experiments, therefore the mass flow through the downstream rim seal gap is assumed to be zero. Out of that, the rim seal purge mass flow P is calculated by the difference of the measured bypass mass flow B and the measured secondary mass flow S. Figure 1 (right) provides a close-up view of the rotor upstream rim seal geometry used for the present investigation. The characteristic geometrical details are the rim seal interface gap width of 20% of the first stator axial chord as well as a sealing gap of 4% of the stator 1 axial chord. A platform chamfer angle of 45 deg is denoted and builds an angel wing on the rotor-sided rim seal geometry.

The rim seal purge flow injection levels are defined by means of the injection rate (IR) given in the following equation:

$$\text{IR} = \frac{\dot{m}_B - \dot{m}_S}{\dot{m}_{\text{MAIN}}} \cdot 100 \tag{1}$$

Table 1 Operating conditions and geometry specifications

Pressure ratio, $\pi_{1.5}$	$1.65 \pm 0.4\%$	—
Inlet total temperature, $T_{0,\text{in}}$	327.9 ± 0.3	K
Capacity, $\dot{m}\sqrt{T_{0,\text{in}}}/p_{0,\text{in}}$	152.7 ± 0.1	$\text{kg K}^{1/2}\,\text{s}^{-1}\,\text{bar}^{-1}$
Nondimensional speed, $N/\sqrt{T_{0,\text{in}}}$	2.49 ± 0.05	$\text{rps K}^{-1/2}$
Mach number (S1 exit/R exit/S2 exit)	0.53/0.26/0.48	—
Reynolds number (S1/R/S2)	7.1/3.8/5.1	$\times 10^5$
Blade count (S1/R/S2)	36/54/36	—
Aspect ratio (S1/R/S2)	0.87/1.17/0.82	—

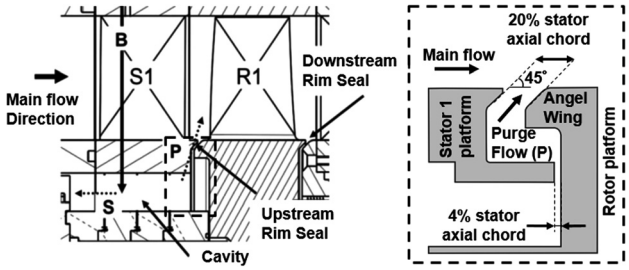

Fig. 1 Schematics of rim seal purge flow path (left) and close-up view of rotor upstream rim seal (right)

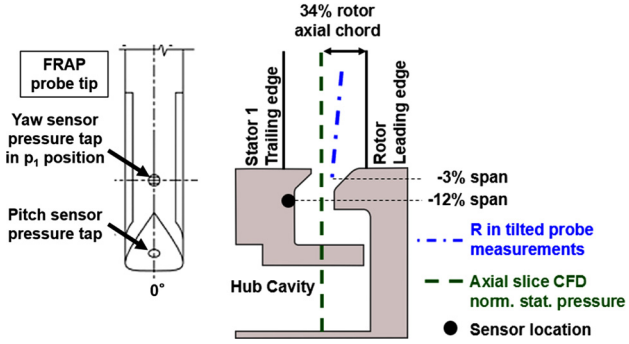

Fig. 2 FRAP probe tip schematic (left) and measurement location (right) of inclined probe measurements R in tilted (dash-dot line) and hub cavity absolute wall pressure transducers (spot). The position of axial slice for CFD normalized static pressure is indicated.

In the present study, experiments for four different injection rates have been conducted: IR0 = 0.0%, IR1 = 0.4%, IR2 = 0.8%, and IR3 = 1.2%, which are representative to real engine conditions.

The IR2 = 0.8% case is termed as the nominal injection rate, whereas IR3 = 1.2% is considered to be the high purge mass flow case. The measurement accuracy of the injected amount of rim seal purge flow with respect to the turbine main mass flow is evaluated to be ±0.01%.

Measurement Technology. In order to measure the unsteady flow field at the interface of the rotor upstream hub cavity, the fast-response aerodynamic probe (FRAP) is used (Fig. 2, left). The probe technology has been developed in-house at LEC at ETH Zurich. Detailed information concerning the measurement technology can be found in Kupferschmied et al. [17] and Pfau et al. [18]. The FRAP allows to measure total and static pressure as well as flow yaw and pitch angle in a frequency bandwidth up to 48 kHz. Based on pressure and flow angle information, the flow velocity components and further flow quantities are derived. For temperature measurements, the frequency bandwidth is limited to 10 Hz. The impact of the measured temperature on the pressure and therefore velocity component is judged to be very modest. In order to reduce the probe blockage effect, the FRAP has a 1.8 mm tip diameter and encapsulates two miniature silicon piezoresistive pressure transducers. The two-sensor FRAP is operated in a virtual four-sensor mode in order to measure the three-dimensional, time-resolved flow properties. The data are acquired at a sampling rate of 200 kHz over a measurement time of 2 s. The postprocessing of the data is performed for six consecutive rotor pitches, which results with the given sampling rate in a flow field temporal resolution of about 82 samples per rotor blade passing event, considering 54 rotor blades and a nominal rotational speed of the rotor of 2700 rpm.

The absolute measurement uncertainties achieved with the FRAP for the rotor upstream hub cavity interface region are given in the subsequent Table 2 for a probe calibration range of ±24 deg in the yaw angle and ±20 deg in the pitch angle. Furthermore, the relative uncertainties of the total (P_0) and static pressure (P_S) are specified as a percentage of the dynamic head. The measurement uncertainty for the total pressure losses Y and the normalized pressure amplitudes are also given.

The probe measurement data presented in this work have been acquired at the rotor upstream hub cavity interface of the axial turbine test section. In order to allow the probe tip to be immersed into the hub cavity, the probe traversing axis toward the turbine axis of rotation has been tilted. Out of that, pressure measurements of the probe's pitch sensor down to −3% blade span have been performed. Due to the inclined probe axis, the axial location of the measurement is changing by traversing to lower spanwise positions. The axial distance of the probe tip to the rotor leading edge when the probe is immersed the most into the hub cavity is 27% of the rotor axial chord. The measurement location is labeled with "R in tilted." The effect of tilting the probe axis in combination with the local high positive flow pitch angles at the rim seal exit has been taken into account in the calibration and data postprocessing. Detailed information on the FRAP aerocalibration scheme for pronounced positive pitch angles can be found in Bosdas et al. [19]. The spatial resolution of the measurement grid consists of 16 points along the tilted probe axis (starting from +30% blade span) and 41 points in circumferential direction covering one stator pitch. The circumferential points are equally spaced whereas for the tilted axis, the clustering has been increased toward the end walls and the hub cavity. In Fig. 2, the concept of the tilted probe axis as well as the lowest accessible spanwise position of the probe is visualized. In addition to the fast-response probe measurements, the hub cavity unsteadiness has been investigated by means of two miniature fast-response absolute wall-mounted pressure transducers based on the FRAP piezoresistive sensor technology. The data are acquired at 200 kHz over a measurement time of 8 s. The absolute pressure sensors have been installed on the stator 1 side cavity wall at −12% blade span. Figure 2 shows the position of the sensors inside the hub cavity.

Computational Setup

In order to complement the time-resolved measurements, unsteady full-annular CFD simulations have been performed in order to provide hub cavity flow field data in regions which have not been resolved by the unsteady flow measurements.

Solver. For this work, the in-house developed computational fluid dynamics (CFD) code MULTI3 has been used which is an unsteady compressible Reynolds-averaged Navier–Stokes (RANS) solver. An explicit, finite-volume, node-based time-marching algorithm developed by Ni provides the base of the solver. The discretization is second-order in both space and time. An anisotropic artificial dissipation algorithm is implemented in order to prevent high-frequency oscillations and capture shock waves. In order to account for the local discrepancy in Courant number in different cell dimensions in the high aspect ratio cells used at the wall, an

Table 2 Uncertainty bandwidth FRAP

Yaw angle (deg)	Pitch angle (deg)	P_0 (%)	P_s (%)	Norm. pressure amplitude	Total pressure loss coefficient, Y (%)
0.62	0.64	1.0	1.2	0.07	0.64

adaptive scaling of the smoothing coefficients is performed. For closure of the RANS equations, a two equation Wilcox k–ω turbulence model is implemented in its low Reynolds number form. In order to speed up the convergence, a local time-stepping approach is used for steady simulations and dual time-stepping for unsteady simulations. The latest version of the code which is running on graphics processing units (GPUs) was used for this study. Detailed information can be found in Refs. [20] and [21].

Mesh and Boundary Conditions. A full-annular mesh for the tested turbine configuration has been generated consisting of the first stator and rotor as well as the rotor upstream hub cavity and blade fillets. The main annulus flow path and the hub cavity have been meshed via the commercial mesh generator "NUMECA Autogrid 5." In order to build up the 360 deg computational model, a 20 deg section model has been meshed, copied, and rotated 17 times for the remaining 340 deg of the full annulus. The total mesh size of the full-annular model is 36×10^6 nodes, presenting a general range of y^+ - values of 1.1 up to 2.3. In order to inject rim seal purge mass flow, a cavity inlet duct is integrated which is representative to the measured turbine configuration. The turbine inlet boundary conditions are taken from probe measurements which have been performed with the same turbine configuration. Inlet total pressure and turbulent intensity level profiles are imposed at the turbine inlet [22,23]. The inlet total temperature is taken constant across the span and equal to the value shown in Table 1. The turbulent length scale at the inlet is assumed to be 5 mm. At the exit of the turbine stage, a radial equilibrium condition is used. Two simulations for the rim seal purge flow rates IR0 = 0.0% and IR2 = 0.8% have been performed in order to better understand the cavity dynamics and the associated flow field.

Results and Discussion

The focus of the current investigation is the unsteady flow field inside and at the interface of a high-pressure gas turbine representative hub cavity. Starting from an experimental and numerical assessment of the flow regime inside the cavity and its characteristic modes, the radial migration of the cavity-induced modes to higher spanwise positions is presented combined with an aerodynamic loss consideration.

Modulation of Turbine Hub Cavity Modes. Several studies have shown hub cavity induced modes that are characterized by a low-frequency content in the pressure spectral analysis which is typically below the rotor blade passing frequency (RBPF). By means of wall-mounted, fast-response pressure transducers, a pressure spectral analysis inside the hub cavity has been performed for four different purge flow injection rate cases. Figure 3 gives the normalized pressure amplitude with respect to the frequency content up to three times the rotor blade passing frequency. In order to compare the findings inside the hub cavity to the radial migration of the hub cavity modes (Radial Migration of Hub Cavity Modes and Aerodynamic Loss Considerations section), the constant normalization factor has been chosen to be the pressure amplitude of the rotor blade passing frequency at 30% span for the IR3 = 1.2% case measured with the FRAP (at 0.5 stator pitch).

For all the four injection rate cases, the presence of the rotor blade passing event ($f/f_{\mathrm{RBPF}} = 1$) is sensed and shows an increase from the lowest considered rim seal purge mass flow IR0 to the highest one, IR3, by a factor of 2.5. The presence of the low-frequency pressure fluctuations below the rotor blade passing frequency can clearly be identified for the injection rates IR0 up to the nominal injection rate case IR2. These low-frequency modes are further on termed with hub cavity modes. The fact that these modes are not defined by one single peak in the pressure spectrum but by a band of frequencies with elevated amplitudes implies that they are not linked to a geometrically triggered acoustic mode. Two characteristic trends are observed for these three cases.

First, the band of frequencies with elevated amplitudes is shifted toward higher frequencies by increasing the purge mass flow. By characterizing these bands by the half-power bandwidth method, the IR0 case reveals a frequency content between 13% and 20% of the rotor blade passing frequency, whereas the IR1 case shows the shift of the spectrum to 21–26% of the RBPF. Furthermore, the IR2 case is defined by a band of frequencies with elevated amplitudes in the range of 25–35% of the RBPF. On the other hand, for the high rim seal purge flow case IR3, no contribution to the pressure spectrum in the low-frequency range is observed. The lack of the cavity mode for IR3 indicates a stabilization effect of pressure fluctuations inside the hub cavity by providing a sufficiently high purge mass flow. In addition, the measurements performed in the range of 0.0–0.8% injection rate suppose that these modes are driven by a mass flow exchange between hub cavity and main annulus flow, meaning that both local injection and ingestion need to take place in order to trigger these modes.

A second trend is observed in terms of pressure amplitude which shows that the hub cavity associated fluctuations are dominant with respect to the rotor blade passing amplitude for the two injection rate cases IR0 = 0.0% and IR1 = 0.4%. Specifically, IR1 shows a pronounced resonance which is double as high as the measured rotor blade passing fluctuations. By further increasing the rim seal purge flow to IR2, the dominance of the cavity mode is weakened and disappears completely when the cavity pressure fluctuation stabilization occurs (IR3).

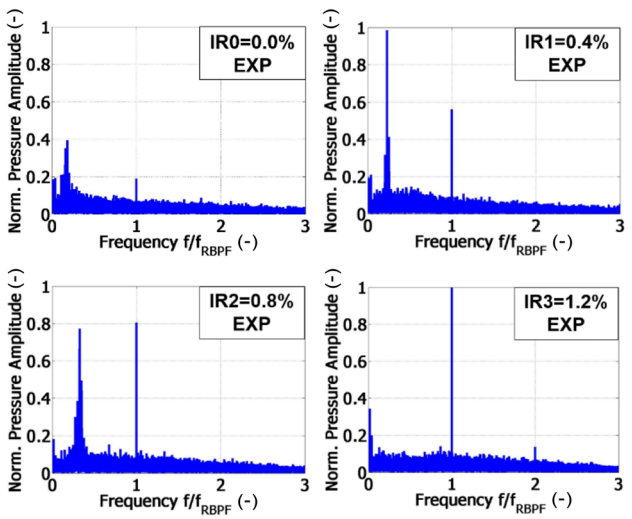

Fig. 3 Experimentally determined pressure frequency spectra for four different injection rate cases inside the hub cavity at −12% span

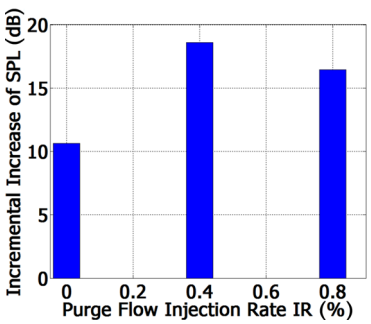

Fig. 4 Measured incremental increase of sound pressure level SPL (dB) induced by the cavity modes with respect to the suppressed cavity mode case IR3 = 1.2% inside the hub cavity

A strong dependency of the hub cavity induced modes on the injected purge mass flow has been identified with respect to frequency content and pressure amplitude. Considering the acoustic characteristics, these cavity modes are within the human perception of sound (frequency range 13–35% of RBPF). The modulation of the amplitude of the cavity mode pressure fluctuations provoked by the different purge flow rates is transferred into a change in the noise level. Figure 4 depicts the measured incremental increase of the sound pressure level (SPL) for IR0 up to IR2 with respect to the IR3 case where the cavity modes are suppressed.

The presence of the cavity modes has a significant impact on the noise level with an increase up to 18 dB for IR1 = 0.4% compared to the operating point IR3 = 1.2%. Even in the absence of purge flow, an increase of the noise level of 11 dB has been found. Given the presented measurements, the order of magnitude in noise reduction that is achieved by suppressing the cavity modes is substantial and shows the non-negligible noise contribution of the cavity modes to the overall noise level of a high-pressure turbine.

In order to further investigate the source of the hub cavity modes, the experimental work is complemented by full-annular unsteady CFD simulations for two injection rates. Figure 5 shows the predicted pressure spectral analysis at the representative location of the unsteady pressure transducers (−12% span, Fig. 2) in order to compare the predicted cavity dynamics to the experiments. The presented spectra as well as all the subsequently shown flow quantities were evaluated after four rotor revolutions. The results show that the simulation is able to predict the dominant cavity mode for the IR0 = 0.0% case. The IR0 band of frequencies with elevated amplitudes of 13–20% of the RBPF is predicted by CFD and also present in the measurement data. However, the simulation provides in addition a broad band of frequencies with elevated amplitudes between the dominant cavity mode and the rotor blade passing frequency (frequency range 42–86% of RBPF). The IR0 amplitude of the dominant cavity mode is overpredicted by a factor of 2.5, whereas the rotor blade passing related pressure fluctuations are overpredicted by a factor of 1.5.

The pressure frequency spectrum for the IR2 = 0.8% case also captures the experimentally predicted frequency content and the shift toward higher frequencies. The simulation shows that the cavity mode is shifted to a frequency band in the range of 27–51% of the RBPF. Therefore, the simulation predicts a broader range of frequencies compared to the experiments. The dominant cavity mode pressure amplitude is overpredicted by a factor of 2.4, whereas the rotor blade passing related pressure amplitude is underpredicted by a factor of 1.3.

Since the dominant effects of the cavity modes are captured, a qualitatively investigation of the flow field inside the hub cavity is valid in order to investigate the source of the low-frequency content. In Fig. 6, the normalized static pressure between the first stator and rotor is shown by means of an axial slice for IR0 = 0.0% and IR2 = 0.8%. The pressure information given is normalized by the turbine inlet total pressure. The depicted slice is located rotor

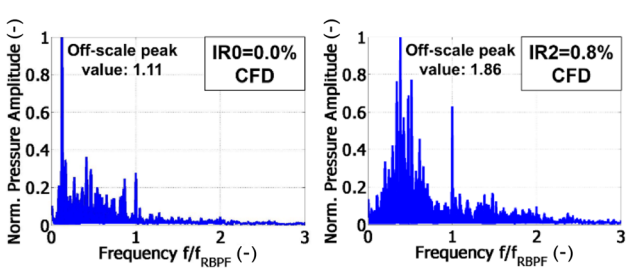

Fig. 5 Predicted pressure frequency spectrum for two rim seal purge flow injection rates at −12% span inside the hub cavity: IR0 = 0.0% (left) and IR2 = 0.8% (right)

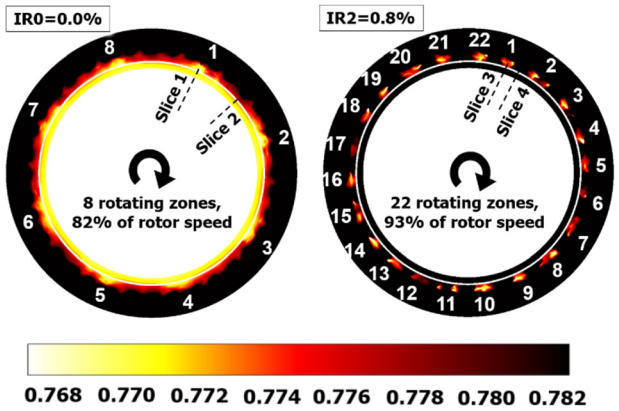

Fig. 6 Instantaneous map of predicted normalized static pressure (-) over the full-annulus for IR0 = 0.0% and IR2 = 0.8%, indication of 8 (IR0 = 0.0%) and 22 (IR2 = 0.8%) low static pressure zones inside the hub cavity

upstream at 34% of the rotor axial chord upstream of the rotor leading edge (Fig. 2). The results show pronounced regions of low static pressure distributed over the circumference (Fig. 6, indices 1–8 (IR0 = 0.0%) and 1–22 (IR2 = 0.8%)). The number of low static pressure zones shows strong sensitivity to the amount of injected rim seal purge flow. IR0 shows 8 pronounced low static pressure zones, whereas IR2 reveals 22 zones around the circumference. The core of these regions shows a reduction in static pressure up to 0.7% compared to the circumferential average in the cavity. A low static pressure suggests that the level of ingestion from the main annulus flow into the hub cavity is increased due to the pronounced radial pressure gradient.

The low static pressure zones were found to rotate with the rotor at a rotational speed of 82% (IR0) and 93% (IR2) of the rotational speed of the rotor. Therefore, a stationary pressure monitoring point inside the cavity experiences these low pressure zones with a frequency of 13.8% (IR0) and 37.9% (IR2) of the RBPF which is in agreement with the band of frequencies with elevated

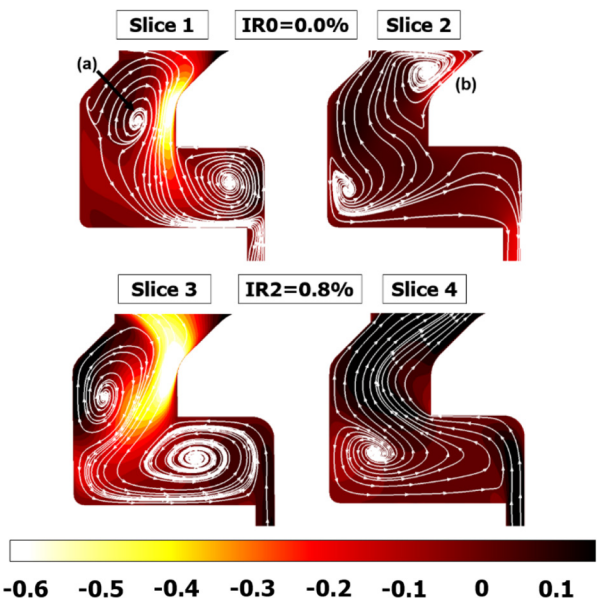

Fig. 7 Close-up view of meridional slice through local low static pressure zone (slices 1 and 3, left) and between two low pressure zones (slices 2 and 4, right) for IR0 and IR2 superimposed with normalized radial velocity contour (-) and hub cavity stream lines

amplitude in the predicted and measured pressure frequency spectrum. The spectral analysis suggests a characteristic time scale of the peak ingestion of hot gas into the cavity in the absence of purge flow. Furthermore, the presence of the low-frequency pressure fluctuations implies that ingestion of hot gas into the cavity is still taking place and gives therefore an appropriate measure of ingestion behavior to the turbine designer plus a judgement whether the amount of purge mass flow is sufficient in order to suppress ingestion. In case of the IR0 = 0.0%, the presence of the first stator S1 is also captured inside the hub cavity which is characterized by 36 zones of low static pressure around the circumference.

In order to understand the source of the low static pressure zones, the flow field inside the hub cavity needs to be further investigated. Figure 7 shows the close-up view of four meridional slices that provide the normalized radial velocity inside the hub cavity superimposed with the projected streamlines. The radial velocity has been normalized by the tangential velocity of the rotor at the hub. The first slice (Fig. 7, slice 1) is radially aligned with the core of the low static pressure zone (index 1). The normalized radial velocity contour clearly shows a pronounced zone of negative radial velocity which describes that flow is going toward the axis of the machine with a velocity up to 60% of the rotor hub tangential velocity. The high negative radial velocity component is induced by the shape of the rim seal which locally accelerates the flow. On the other hand, the presence of the vortical structure (Fig. 7, slice 1, vortex (a)) reduces the effective flow cross section significantly and leads to local acceleration. The center of this vortex is found to be at the same radial position as the most pronounced region of the negative radial velocity.

Consequently, the pronounced negative radial velocity zone and therefore the low static pressure zone are triggered by the vortical structures and the shape of the rim seal. The results imply that the center of the vortex needs to have a certain radial position and spatial extent, meaning that the axial width of the vortex needs to be in the order of magnitude of the gap between stator sided cavity wall and the rotor angel wing (around 20% of the stator 1 axial chord). Due to the fact that the hub cavity flow structures undergo a modulation in time and along the circumference which is also depicted in Fig. 7 in slice 2, the cavity mode is associated to a vortex modulation and formation. The contour plot shows that the radial velocity is increased toward positive values and the vortex radially migrates toward the exit of the rim seal (Fig. 7, slice 2, vortex (b)). Similar findings are identified by considering the IR2 = 0.8% case. The radial position of the vortex core also for this case affects the radial velocity distribution inside the hub cavity (Fig. 7, slice 3), whereas in regions in between the low pressure zones only purging occurs (Fig. 7, slice 4).

The findings of the experimental data and numerical predictions imply that similar mechanisms occur for low and moderate purge flow injection rates. For high purge flow injection rates IR3 = 1.2%, the signature in the pressure frequency spectrum disappears which suggests that for triggering the modes, both injection and ingestion need to take place. If only injection occurs, the cavity mode is suppressed.

Radial Migration of Hub Cavity Modes and Aerodynamic Loss Considerations. The investigation inside the hub cavity suggests that the cavity modes are defined by a local mass flow exchange between cavity and main annulus flow. The migration of these effects toward higher spanwise positions is analyzed.

Of specific interest is the tracing of the flow unsteadiness generated by the purge flow entrainment and mass flow exchange process between cavities and main annulus flow. Schuepbach et al. [8] showed that purge flow mixing and migration have a pronounced impact on the local unsteadiness of the flow field. The rms values of the random part of the time-resolved pressure signal $p'(t)$ acquired by FRAP provide an indication of the unsteadiness present in the flow field. Based on the triple pressure decomposition [24] shown in Eq. (2), the random part is calculated by the difference of the time-resolved signal $p(t)$ and the phase-locked averaged pressure signal $\bar{p} + \tilde{p}(t)$

$$p(t) = \bar{p} + \tilde{p}(t) + p'(t) \tag{2}$$

In order to identify regions of high flow unsteadiness, the time-averaged rms (stochastic consideration) of the random part of the pressure signal of the center yaw pressure tap $p'_1(t)$ of the FRAP is shown in Fig. 8 for IR2 and IR3 and up to 30% span. By comparing the two purge flow injection cases, a clear increase of the unsteadiness level is observed. Especially around 0.5 stator pitch and toward 1% blade span, the region of purge flow intrusion into the main annulus flow is identified. Furthermore, the injection of additional purge mass flow IR3 is not only intensifying the local flow unsteadiness, but also showing more spreading of unsteadiness around the circumference in close vicinity to the hub. The relative change of rms $p'_1(t)$ in Fig. 8(*c*) underlines this observation, showing that the increase of stochastic unsteadiness in close vicinity to the hub reaches up to 40% when increasing the rim seal purge flow from IR2 = 0.8% to IR3 = 1.2%.

Based on these findings, the assessment of migrating hub cavity modes should be focused on the region around 0.5 stator pitch where the highest transport of cavity fluid into the main annulus flow is taking place. This location is insensitive to the injected amount of purge flow which has also been reported by Jenny [25] and specified that the upstream located nozzle guide vane defines where the purge flow is leaving the rim seal hub cavity.

In addition to that, both injection rate cases show an increased unsteadiness in the region at 10% span and 0.4 stator pitch which is induced by the stator 1 hub passage vortex (HPV) and trailing edge shed vortex (TESV). The traces of these secondary flow structures are depicted in Fig. 9 by means of measured time-averaged axial vorticity for the injection rates IR2 and IR3. The stator 1 hub passage vortex is characterized by regions of pronounced negative axial vorticity at around 0.4 stator pitch and 6% span. The trailing edge shed vortex, on the other hand, shows pronounced positive axial vorticity at 0.5 stator pitch and 15% span.

It is remarkable that the region of the purge flow injection from the hub cavity into the main annulus and the circumferential

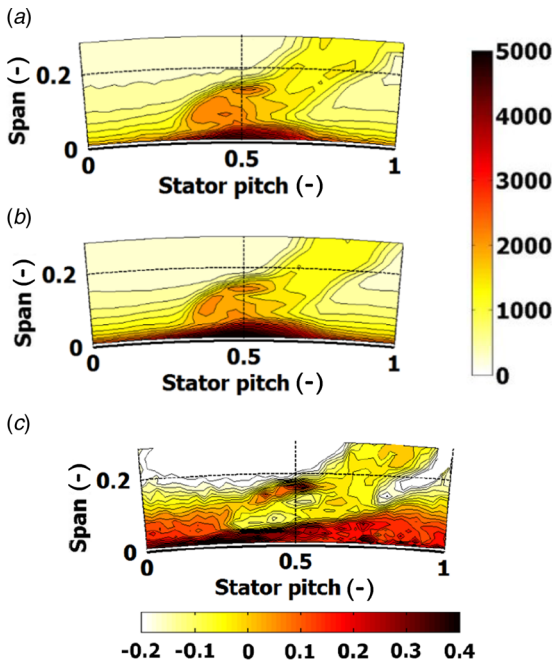

Fig. 8 Time-averaged rms of p'_1 (Pa) in stationary frame of reference at R in tilted plane: (*a*) IR2 = 0.8%, (*b*) IR3 = 1.2%, and (*c*) relative change of rms p'_1 (-) by increasing IR2 to IR3

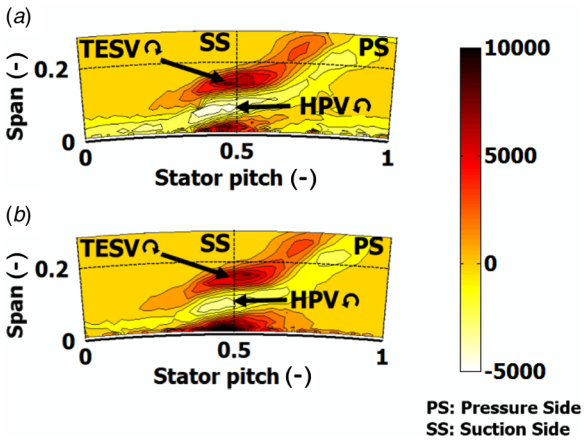

Fig. 9 Time-averaged axial vorticity (Hz): (*a*) IR2 = 0.8% and (*b*) IR3 = 1.2%. Indication of secondary flow structures: trailing edge shed vortex (TESV) and stator 1 hub passage vortex (HPV).

position of the secondary flow structures is aligned radially. This implies that the presence of the HPV and TESV benefits the intrusion of the purge flow.

Based on the presented measurements, a radial spectral analysis of the flow field has been performed starting from −3% span up to +30% span using the measured absolute pressure of the FRAP pitch pressure sensor.

The circumferential position is kept constant at 0.5 stator pitch where most of the injected rim seal purge flow leaves the hub cavity and penetrates into the main annulus flow. In Fig. 10, three spectral analysis plots are shown for IR2 = 0.8% and IR3 = 1.2%,

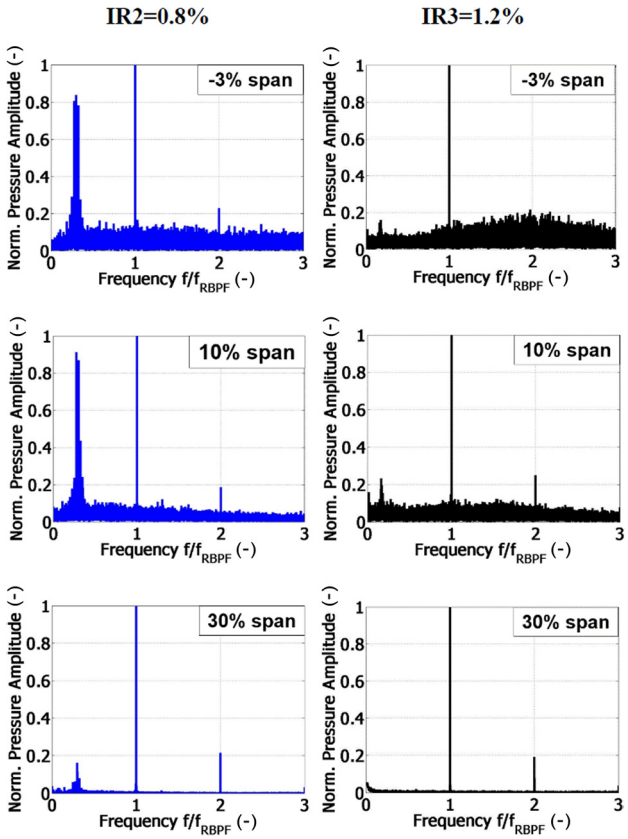

Fig. 10 Pressure spectral analysis at three spanwise positions and stator pitch 0.5 for rim seal purge flow IR2 = 0.8% (left column, left) and IR3 = 1.2% (right column)

respectively. The frequency is presented in terms of the rotor blade passing frequency RBPF, and the pressure amplitude is normalized by the pressure amplitude induced by the rotor blade passing for the IR3 = 1.2% case at 30% span. The fast Fourier transformation (FFT) of the measured absolute pressure shows clearly three frequencies with elevated amplitudes for the IR2 = 0.8% case, whereas two of them are related to the rotor blade passing defined by the first and second harmonics. For all the three spanwise positions, the rotor blade passing event ($f/f_{RBPF} = 1$) shows the highest amplitude across the spectrum. However, the band of frequencies with elevated amplitudes in the range of 25–35% of RBPF reaches up in pressure amplitude to 84% of the dominant frequency at −3% span and even 91% at 10% span. This frequency content is in the same range as the wall-mounted pressure transducers at −12% span have shown. Furthermore, it can be stated that the dominance of rotor blade passing effects is broken up by the presence of the cavity resonances. In other words, the interaction mechanisms for the flow field at the rim seal exit take place at two different characteristic time scales which are defined by the rotor blade passing period (fast) and the cavity mode induced period (slow).

The measurements indicate that the presence of the stator 1 hub passage vortex and trailing edge shed vortex (region around 10% span) does not lead to a change of the cavity-induced frequency content but intensifies the strength of the pressure fluctuations. After crossing the unsteadiness of the secondary flow structures toward 30% span, a clear reduction of the pressure amplitude by a factor of 5 peak-to-peak is observed. Still at 30% blade span, the signature of the hub cavity originated resonances is present and in the same order of magnitude as the second harmonic of the rotor blade passing ($f/f_{RBPF} = 2$). The IR3 case in Fig. 10 reveals that the cavity-induced pressure fluctuations are significantly reduced compared to the previous case. Considering the low-frequency range at −3% span, a moderate signature of a cavity mode is suspected in the range of 14–20% of the rotor blade passing frequency.

In this frequency band, the presence of the secondary flow structures is again enhancing the strength of the pressure fluctuations and not shifting the frequencies. However, the level of the pressure fluctuations defined by the cavity modes is by a factor of 4 lower than for the IR2 = 0.8% case. The signature of the cavity mode is completely vanished at 30% blade span. Together with the results provided by the wall-mounted pressure transducers at −12% span, the presented data underline the phenomena of a stabilization of the pressure fluctuations inside the hub cavity by increasing the purge mass flow to IR3 = 1.2%.

In addition to the previous considerations, the cavity-induced modes are related to a change in aerodynamic losses. A total pressure loss coefficient is introduced in order to quantify the losses at the rim seal exit including the present secondary flow structures

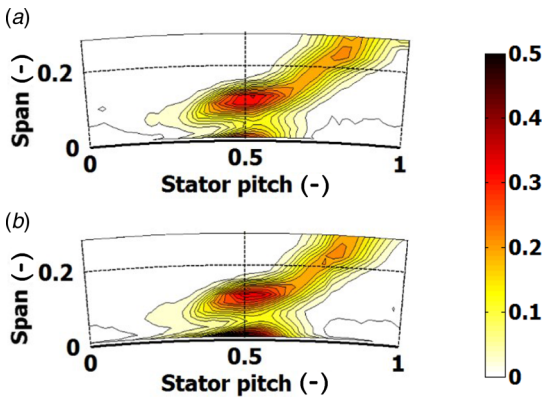

Fig. 11 Time-averaged total pressure loss coefficient *Y* (-) in stationary frame of reference at R in tilted plane: (*a*) IR2 = 0.8% and (*b*) IR3 = 1.2%

(HPV and TESV). Equation (3) provides the definition of the coefficient which normalizes the measured absolute total pressure loss with the dynamic head at the exit of the first stator

$$Y = \frac{p_{0,\text{in}} - p_{0,S1,\text{exit}}}{p_{0,S1,\text{exit}} - p_{s,S1,\text{exit}}} \tag{3}$$

In Fig. 11, the measured time-averaged total pressure loss coefficient is depicted for two injection rate cases. The contour plot covers one stator pitch and reaches up to 30% span in order to emphasize the losses at the rim seal exit.

Both purge flow injection rate cases reveal two regions of highest total pressure loss where one is located at 10% span where the hub passage vortex and the trailing edge shed vortex are interacting. Comparing both injection rate cases, the high purge flow case IR3 shows locally an time-averaged increase of the total pressure losses in this region of 1.9%. Although, the total pressure losses are enhanced by the increased purge flow, the radial location of the total pressure loss core is not affected.

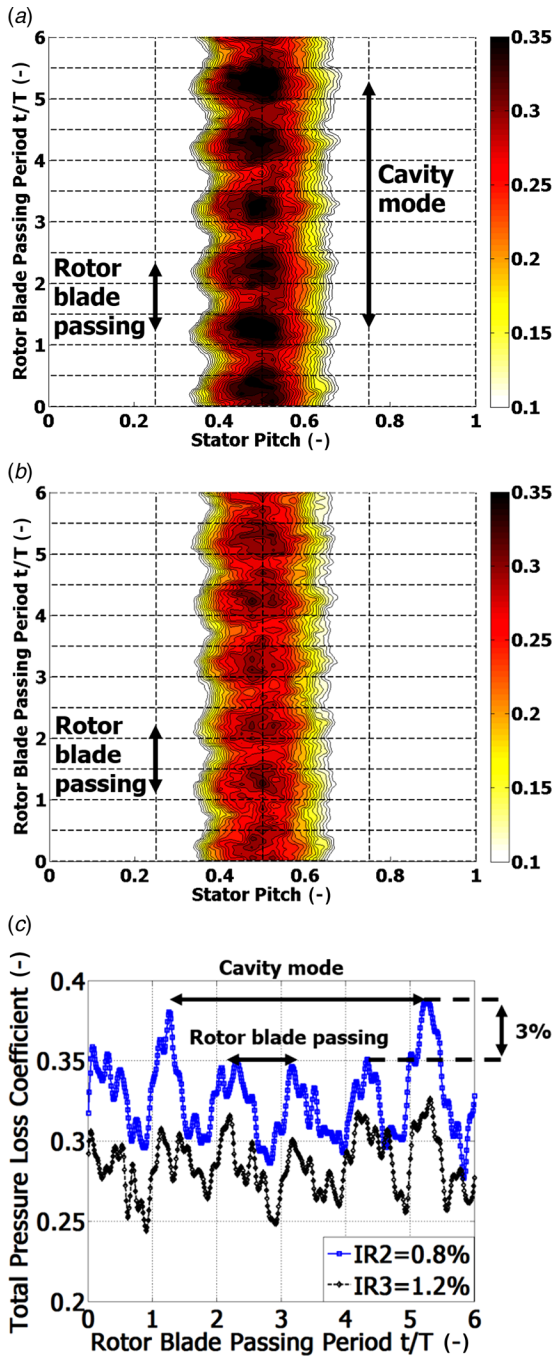

Fig. 12 Space time plot of total pressure loss coefficient *Y* (-) at 10% blade span: (*a*) IR2 = 0.8%, (*b*) IR3 = 1.2%, and (*c*) 2D representation at 0.5 stator pitch and 10% span for six consecutive rotor blade passing events

The most pronounced region of total pressure loss is measured in close vicinity to the hub region (1% span) around 0.5 stator pitch where also the highest flow unsteadiness has been found and identified as location of highest purge flow entrainment into the main annulus flow. In the core of this unsteadiness, a significant increase of total pressure loss of 19.3% is associated when changing the purge mass flow from IR2 = 0.8% to IR3 = 1.2%. Compared to the total pressure loss core induced by the HPV and TESV (Fig. 11, 0.5 stator pitch and 10% span), the region of cavity fluid intrusion shows clear sensitivity in its radial and circumferential spreading to the amount of injected purge flow. Similar to the flow unsteadiness, the total pressure loss regions spread more in radial and circumferential directions for higher purge flow in close vicinity to the hub.

A time-averaged consideration of aerodynamic losses is not sufficient since the presence of the low-frequency modes asks for a time-resolved investigation. Figure 12 provides a time and space resolved plot of the total pressure loss coefficient *Y* for two purge flow injection rate cases IR2 and IR3. The radial position of the time-averaged total pressure loss core (10% span) has been chosen due to the strong presence of the cavity mode for IR2 = 0.8% (Fig. 10). The time axis covers six consecutive rotor blade passing events. Both cases show a change in total pressure loss with respect to the rotor blade passing events. Furthermore, Fig. 12(c) provides a cut through the circumferential position 0.5 stator pitch at 10% blade span which implies that another characteristic time scale is present that modulates the time-resolved total pressure losses for the IR2 = 0.8% case. An increase of 3% in total pressure losses compared to the rotor blade passing induced losses can be observed.

This implies that another loss mechanism needs to be present in addition to the impact of varying the purge flow injection. Considering Fig. 10, a clear difference in the pressure frequency spectrum in terms of low-frequency modes has been identified between IR2 and IR3. Specifically, the IR2 case at 10% span shows a frequency content of 25–35% of RBPF which supposes that a certain event occurs every fourth blade passing event.

Figures 12(*a*)–12(*c*) present this behavior where two pronounced loss events are separated in time by four blade passing events which are associated to the low-frequency cavity mode of the IR2 case. The strong presence of the loss core is generated by the superposition of the rotor blade passing and the cavity mode since the appearance of the cores seems to be in phase.

The results imply that the presence of these low-frequency cavity modes is a source of aerodynamic losses, which increases the detrimental impact of the total pressure loss core and shifts the total pressure losses of the nominal purge flow injection rate case closer to a turbine operational point with higher injection of rim seal purge flow. The benefit in loss reduction by injecting a lower amount of purge mass flow is therefore weakened by the hub cavity induced modes.

Conclusions

This paper presents results of an experimental and numerical investigation of the turbine hub cavity modes. Time-resolved measurements and unsteady full-annular simulations have shown the potential to identify these modes and relate them to flow mechanisms as well as noise emissions and aerodynamic losses.

Specifically, clear turbine hub cavity induced modes have been identified, which tend to migrate up to 30% blade span. These modes are characterized by low-frequency pressure fluctuations which strongly depend on the amount of injected rim seal purge flow, both in amplitude and frequency content. The pressure

frequency spectrum reveals that these modes are within the human perception of sound and provide a non-negligible contribution to the noise emission of a high-pressure turbine. A significant reduction of the cavity-induced noise is achieved by injecting a sufficient amount of rim seal purge flow (IR3 = 1.2%), which leads to a stabilization of the pressure fluctuations.

Full-annular unsteady RANS simulations show the potential of predicting the cavity-induced modes and confirm that the low-frequency modes are related to pronounced and spatially distinct ingestion and injection spots around the circumference which rotate with the rotor. Consequently, as long as the low-frequency hub cavity modes are present, the turbine designer has to expect local high static pressure gradients which define the level of ingestion of hot gas into the turbine hub cavity.

The presence of the hub cavity modes has been linked to an aerodynamic loss mechanism. Measurements radially aligned with the loss core induced by the hub passage vortex and trailing edge shed vortex for the nominal injection rate case IR2 = 0.8% underline that pronounced zones of high total pressure loss occur in time defined by the dominant cavity mode frequency. A comparison with the high injection rate case IR3 = 1.2% shows that the losses for IR2 = 0.8% in the hub passage vortex core are increased up to 3% every fourth blade passing event. The benefit in loss reduction by reducing the purge mass flow is therefore weakened by the hub cavity induced modes.

The findings of this work stress the fact that the hub cavity induced modes need to be taken into account in the turbine design process with specific aim of stabilizing the cavity dynamics in order to lower the noise emission and reduce the aerodynamic losses for turbine operating points with nominal and moderate rim seal purge flow injection rates.

Acknowledgment

The authors gratefully acknowledge the permission of Siemens and MTU to publish the data and the financial and intellectual support during the measurements. The support of Dominic Hänni, Ilias Papagiannis, Asad Raheem, and Andrea Mazzetti from the Laboratory for Energy Conversion at ETH Zurich for the help in setting up the numerical predictions is gratefully acknowledged.

Nomenclature

f = frequency (Hz)
IR = rim seal purge flow injection rate (%)
$\dot{m}$ = mass flow (kg/s)
N = rotational speed (rpm)
p = pressure (Pa)
$\bar{p}$ = mean-time pressure component (Pa)
$\tilde{p}$ = periodic pressure component (Pa)
p' = random pressure component (Pa)
SPL = sound pressure level (dB)
T = temperature (K)
Y = total pressure loss coefficient
y^+ = nondimensional wall distance
π = pressure ratio

Subscripts

c = compressor
in = turbine inlet flow quantity
s = static flow quantity
0 = stagnation flow quantity
1.5 = one-and-a-half stage

Abbreviations

CFD = computational fluid dynamics
CFL = Courant number
EXP = experiments
FFT = fast Fourier transformation
FRAP = fast-response aerodynamic probe
GPU = graphics processing unit
HPV = hub passage vortex
PS = pressure side
RANS = Reynolds-averaged Navier–Stokes
RBPF = rotor blade passing frequency
SS = suction side
S1 = first stator
S2 = second stator
TESV = trailing edge shed vortex

References

[1] Johnson, B. V., Mack, G. J., Paolillo, R. E., and Daniels, W. A., 1994, "Turbine Rim Seal Gas Path Flow Ingestion Mechanisms," AIAA Paper No. 94-2703.
[2] Popović, I., and Hodson, H. P., 2013, "The Effects of a Parametric Variation of the Rim Seal Geometry on the Interaction Between Hub Leakage and Mainstream Flows in High Pressure Turbines," ASME J. Eng. Gas Turbines Power, **135**(11), p. 112501.
[3] Popović, I., and Hodson, H. P., 2010, "Aerothermal Impact of the Interaction Between Hub Leakage and Mainstream Flows in Highly-Loaded HP Turbine Blades," ASME J. Eng. Gas Turbines Power, **135**(6), p. 061014.
[4] Julien, S., Lefrancois, J., Dumas, G., Boutet-Blais, G., Lapointe, S., Caron, J.-F., and Marini, R., 2010, "Simulations of Flow Ingestion and Related Structures in a Turbine Disk Cavity," ASME Paper No. GT2010-22729.
[5] Boudet, J., Hills, N. J., and Chew, J. W., 2006, "Numerical Simulation of the Flow Interaction Between Turbine Main Annulus and Disc Cavities," ASME Paper No. GT2006-90307.
[6] Jakoby, R., Zierer, T., DeVito, L., Lindblad, K., Larsson, J., Bohn, D. E., Funcke, J., and Decker, A., 2004, "Numerical Simulation of the Unsteady Flow Field in an Axial Gas Turbine Rim Seal Configuration," ASME Paper No. GT2004-53829.
[7] Chilla, M., Hodson, H. P., and Newman, D., 2013, "Unsteady Interaction Between Annulus and Turbine Rim Seal Flows," ASME J. Turbomach., **135**(5), p. 051024.
[8] Schuepbach, P., Abhari, R. S., Rose, M. G., Germain, T., Raab, I., and Gier, J., 2010, "Effects of Suction and Injection Purge-Flow on the Secondary Flow Structures of a High-Work Turbine," ASME J. Turbomach., **132**(2), p. 021021.
[9] Hunter, S. D., and Manwaring, S. R., 2000, "Endwall Cavity Flow Effects on Gaspath Aerodynamics in an Axial Flow Turbine—Part I: Experimental and Numerical Investigations," ASME Paper No. GT2000-651.
[10] Jenny, P., Abhari, R. S., Rose, M. G., Brettschneider, M., Gier, J., and Engel, K., 2011, "Low-Pressure Turbine End Wall Design Optimisation and Experimental Verification in the Presence of Purge Flow," ISABE Conference, Gothenburg, Sweden, Sept. 12–16, Paper No. ISABE-2011-1717.
[11] Reid, K., Denton, J. D., Pullan, G., Curtis, E., and Longley, J., 2006, "The Effect of Stator-Rotor Hub Sealing Flow on the Mainstream Aerodynamics of a Turbine," ASME Paper No. GT2006-90838.
[12] Mclean, C., Camci, C., and Glezer, B., 2001, "Mainstream Aerodynamic Effects Due to Wheelspace Coolant Injection in a High-Pressure Turbine Stage—Part I: Aerodynamic Measurements in the Stationary Frame," ASME J. Turbomach., **123**(4), pp. 687–696.
[13] Paniagua, G., Dénos, R., and Almeida, S., 2004, "Effect of the Hub Endwall Cavity Flow on the Flow-Field of a Transonic High-Pressure Turbine," ASME J. Turbomach., **126**(4), pp. 578–586.
[14] Ong, J. H. P., Miller, R. J., and Uchida, S., 2012, "The Effect of Coolant Injection on the Endwall Flow of a High Pressure Turbine," ASME J. Turbomach., **134**(5), p. 051003.
[15] Behr, T., Kalfas, A. I., and Abhari, R. S., 2007, "Unsteady Flow Physics and Performance of a One-and-1/2-Stage Unshrouded High Work Turbine," ASME J. Turbomach., **129**(2), pp. 348–359.
[16] Regina, K., Kalfas, A. I., Abhari, R. S., Lohaus, A., Voelker, S., and auf dem Kampe, T., 2014, "Aerodynamic Robustness of End Wall Contouring Against Rim Seal Purge Flow," ASME Paper No. GT2014-26007.
[17] Kupferschmied, P., Köppel, P., Gizzi, W., Roduner, C., and Gyarmathy, G., 2000, "Time-Resolved Flow Measurements With Fast-Response Aerodynamic Probes for Turbomachines," Meas. Sci. Technol., **11**(7), pp. 1036–1054.
[18] Pfau, A., Schlienger, J., Kalfas, A. I., and Abhari, R. S., 2003, "Unsteady 3-Dimensional Flow Measurement Using a Miniature Virtual 4 Sensor Fast Response Aerodynamic Probe (FRAP)," ASME Paper No. GT2003-38128.
[19] Bosdas, I., Mansour, M., Kalfas, A. I., Abhari, R. S., and Senoo, S., 2015, "Unsteady Wet Steam Flow Field Measurements in the Last Stage of Low Pressure Steam Turbine," ASME J. Eng. Gas Turbines Power, **138**(3), p. 032601.
[20] Burdet, A., 2005, "A Computationally Efficient Feature-Based Jet Model for Prediction of Film-Cooling Flows," Ph.D. thesis, Eidgenössische Technische Hochschule Zürich, Zurich, Switzerland, Dissertation ETH No. 16163.
[21] Basol, A. M., Raheem, A., Huber, M., and Abhari, R. S., 2014, "Full-Annular Numerical Investigations of the Rim Seal Cavity Flows Using GPU's," ASME Paper No. GT2014-26755.

[22] Behr, T., 2007, "Control of Rotor Tip Leakage and Secondary Flow by Casing Air Injection in Unshrouded Axial Turbines," Ph.D. thesis, Eidgenössische Technische Hochschule Zürich, Zurich, Switzerland, Dissertation ETH No. 17283.
[23] Laveau, B., Abhari, R. S., Crawford, M. E., and Lutum, E., 2014, "High Resolution Heat Transfer Measurements on the Stator Endwall of an Axial Turbine," ASME J. Turbomach., **137**(4), p. 041005.
[24] Porreca, L., Hollenstein, M., Kalfas, A. I., and Abhari, R. S., 2007, "Turbulence Measurements and Analysis in a Multistage Axial Turbine," J. Propul. Power, **23**(1), pp. 227–234.
[25] Jenny, P., 2012, "Interaction Mechanisms Between Rim Seal Purge Flow and Profiled End Walls in a Low-Pressure Turbine," Ph.D. thesis, Eidgenössische Technische Hochschule Zürich, Zurich, Switzerland, Dissertation ETH No. 20429.